Shevchenko, Andriy; Nyman, Markus; Kaivola, Matti

All-optical modulation and detection using a gain medium in a pulse shaper

Published in:
Optics Express

DOI:
10.1364/OE.408472

Published: 23/11/2020

Document Version
Publisher's PDF, also known as Version of record

Research Article | Vol. 28, No. 24 / 23 November 2020 / Optics Express 35869
Optics EXPRESS

All-optical modulation and detection using a gain medium in a pulse shaper

M. NYMAN,* M. KAIVOLA, AND A. SHEVCHENKO

Department of Applied Physics, Aalto University, P.O.Box 13500, FI-00076 Aalto, Finland
markus.nyman@aalto.fi

Abstract: We demonstrate all-optical modulation and ultrafast detection using an on-resonance optical gain medium, combined with spectral splitting in a Fourier transform pulse shaper. Multiple spectral channels of one optical beam can be independently modulated in time by another beam, allowing high-rate modulation and multiplexing without requiring ultrafast response from the gain medium. For detection of sub-picosecond signals we demonstrate a method of ultrafast signal detection (temporal imaging with no spatial resolution) that utilizes the spatio-temporal tilt of an optical pulse in a pulse shaper. The proposed methods can find applications in optical information technology and ultrafast imaging.

1. Introduction

Sub-picosecond optical waveforms such as pulses from mode-locked lasers enable ultrafast processing and analysis of optical information, a field driven by scientific and technological applications, such as optical signal processing [1] and ultrafast imaging of chemical reactions and laser-induced phenomena [2,3]. These pulses provide the speed and intensity required for efficient photon-photon interaction mediated, e.g., by nonlinear optical media. In particular, this permits all-optical modulation, that is, modifying optical signals with other optical signals. One of the "holy grails" of this research field would be demonstration of continuous, THz-bandwidth, large-depth all-optical modulation with modest power requirements. Progress towards this goal has been made, though typically there are significant tradeoffs between modulation speed, depth, power requirements, and the size of the device. The fastest all-optical modulation methods rely either on nonlinear effects such as two-photon absorption and Kerr effect, or intraband transitions in semiconductors, strengthened by microcavity resonances [4–7]. Four-wave-mixing-based optical processing in nonlinear waveguides is also common, though mostly used for other processing tasks than modulation [8]. Furthermore, there are optical phenomena (such as free-carrier excitation [9]) that can be used to switch between states rapidly but require a long relaxation period, thus not being capable of continuous ultrafast modulation.

Meanwhile, to *analyze* ultrafast optical information, it needs to be demodulated from the optical signal in a way that allows detection by relatively slow optoelectronic devices. Often this involves division of the signal into its frequency components that can be handled separately. A venerable example is wavelength-division multiplexing in fiber-optic communications, and its recent evolutions such as frequency-comb-based multiplexing [10]. In ultrafast imaging, the wavelength components of a femtosecond pulse can be mapped into different arrival times at an object, and also to different spatial locations, thereby permitting slow array detectors to resolve fast phenomena [2,3,11]. These principles are also utilized in pulse shapers, devices in which amplitude or phase masks (typically provided by spatial light modulators) are used as spectral filters to produce desired changes in the time domain behaviour of an optical field [12,13].

In this work, we demonstrate a theoretical and experimental proof of principle of spectrally-resolved all-optical modulation and multiplexing in an on-resonance optical gain medium combined with a Fourier transform pulse shaper [13,14]. The pulse shaper consists of two gratings and lenses (see Fig. 1) that are used to split an optical beam into its spectral components

#408472 https://doi.org/10.1364/OE.408472
Journal © 2020 Received 26 Aug 2020; revised 20 Oct 2020; accepted 4 Nov 2020; published 11 Nov 2020

Optics EXPRESS

and then join them into a single beam again. With the pulse shaper, multiple spectral components of a signal beam derived from a mode-locked laser can be addressed independently. Unlike in usual pulse shapers where static masks or electronically-controlled spatial light modulators are used [13,15–17], we use an optical gain medium. This permits all-optical modulation by pump-induced population changes in the gain medium, leading to switching-type modulation of the signal transmission either by changing absorption or by amplification. The spectral components are each modulated at a rate determined by the repetition rate of the laser, but due to the wavelength multiplexing the overall modulation rate is a multiple of the repetition rate. The modulation, being based on on-resonance transitions, is also relatively strong compared to off-resonance nonlinear optical effects, and requires no resonator enhancement. The proposed device thereby works as both an all-optical *multiplexer*, when each wavelength component is independently modulated, and an optically addressed *pulse shaper* capable of sub-picosecond modulation. We predict that this method can be further developed to achieve overall multi-THz bandwidth and create also integrated all-optical modulators and detectors.

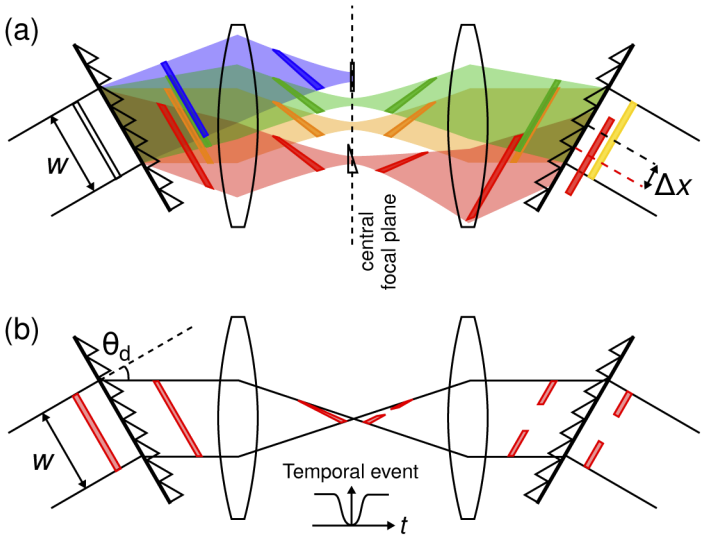

Fig. 1. The Fourier transform pulse shaper consisting of two transmissive gratings and two lenses. The wavelength-splitting function of the pulse shaper (utilized in all-optical modulation) is shown in (a), where the pulse shaper is used to delay the red frequency component and block the purple one. The coloured rectangles represent the position of the pulse at different times. The space-to-time mapping function (used in detection) is shown in (b), where a temporal event consisting of a short dip in transparency modulates the spatio-temporally tilted pulse.

In addition to allowing for spectral control of pulses, the Fourier transform pulse shaper acts as a space-to-time and time-to-space transformer [18]. We use this transformation property to demonstrate a ultrafast *signal detection* method. A femtosecond pulse has a spatiotemporal tilt in the pulse shaper, manifesting itself as a spatially varying time delay, which can be used to probe a time-varying object inserted into the central focal plane of the pulse shaper. We experimentally demonstrate sub-picosecond time resolution in a multi-picosecond burst, which can be used in ultrafast detection and measurement applications. Compared to time-lens-based systems capable of the same [19], our setup is remarkably simple, being implementable with just a mode-locked laser and a few optical components.

Optics EXPRESS

In the paper, Section 2 provides a theoretical analysis of the modulation mechanism and the optical system (in both all-optical modulation and detection). Section 3 presents the experimental results. In Section 4, we make concluding remarks.

2. Modulation mechanism and optical system

2.1. Gain medium for all-optical modulation

The absorption coefficient of an optical gain medium changes upon excitation by a short pump pulse. In transient absorption spectroscopy, the resulting change in the absorption coefficient $\alpha(\lambda)$ at vacuum wavelength λ is typically divided into three parts as follows:

$$\Delta\alpha(\lambda) = \Delta\alpha_{\mathrm{depl}}(\lambda) + \Delta\alpha_{\mathrm{stim}}(\lambda) + \Delta\alpha_{\mathrm{ESA}}(\lambda), \tag{1}$$

where $\Delta\alpha_{\mathrm{depl}}(\lambda)$ is the change by the depletion of the ground state population (also known as "ground state bleach", not to be confused with photochemical bleaching), $\Delta\alpha_{\mathrm{stim}}(\lambda)$ is the change by the onset of stimulated emission, and $\Delta\alpha_{\mathrm{ESA}}(\lambda)$ is the change by the onset of excited-state absorption [20]. The ground-state depletion and stimulated emission terms are negative, while the excited-state absorption term is positive. All-optical modulation can be realized using any of these changes, though here we concentrate on the ground-state depletion and stimulated emission. Simply put, a pump pulse *switches* the absorption coefficient to a different value, changing thus the transmitted power of a probe pulse ($P = P_{\mathrm{inc}} \exp(-\alpha d)$ in a medium of thickness d, where P_{inc} is the incident power). This allows one to realize all-optical amplitude modulation. We note that the refractive index of the medium typically changes during pumping as well, which causes phase modulation, but we ignore this effect here [9,21].

To obtain an approximate theoretical description of the depletion-based modulation we use a two-level atom model, in which Rabi oscillations and spontaneous emission are neglected during the pump pulse. If a thin slice of the gain medium is pumped with a pump pulse of fluence (pulse energy per area) Γ_{p}, the population density attained in the upper level is [22]

$$N_2 = \frac{N_0}{2}\left[1 - \exp\left(-\frac{2\Gamma_{\mathrm{p}}\sigma_{12}}{\hbar\omega_{\mathrm{p}}}\right)\right], \tag{2}$$

where N_0 is the density of molecules, σ_{12} is the absorption cross section, and $\hbar\omega_{\mathrm{p}}$ is the pump photon energy. This translates to

$$\Delta\alpha = -2N_2\sigma_{12}, \tag{3}$$

which we can use to select an appropriate density for the molecules at a given fluence of the pump pulse. The factor of 2 in this equation reflects the fact that, in the two-level system, stimulated emission following the absorption process doubles the change in transparency of the gain medium.

While the excitation of the molecules can be fast, their decay back to the ground state is typically slow and not suitable for sub-picosecond modulation alone. In the following, we will show that when a pulse shaper is utilized to address individual wavelength components, the slow decay is not an issue.

2.2. Fourier transform pulse shaper

The Fourier transform pulse shaper is illustrated in Fig. 1(a) from the point of view of its wavelength-splitting characteristics. It is composed of a grating that maps wavelength to propagation direction, a lens that focuses the spectrally dispersed beam, and then another lens and grating to revert this operation. Any transparency placed on the central focal plane performs spectral filtering. The device has been analyzed previously in detail [14,18] and we present

Optics EXPRESS

here only the most relevant results. At the central focal plane, the spectrum appears as mapped between the transverse coordinate x and the wavelength,

$$x = \frac{(\lambda - \lambda_c)L}{\Lambda \cos(\theta_d)}, \tag{4}$$

where λ_c is the central wavelength, Λ is the period of the grating, θ_d the diffraction angle and L is the focal length. The spectral resolution is given by

$$\Delta\lambda = \frac{\Lambda \cos(\theta_d)}{w}\lambda_c, \tag{5}$$

where w is the width of the incident beam. In terms of all-optical modulation, the spectral resolution determines how many spectral components one can modulate independently from each other. The temporal pulse width at the focal plane is

$$T = \frac{w\lambda_c}{c\Lambda \cos(\theta_d)} = \frac{w \sin(\theta_d)}{c \cos(\theta_d)}, \tag{6}$$

where c is the speed of light. T is normally significantly longer than the original pulse width. The additional width essentially originates from the fact that the input pulse is spatio-temporally tilted by the first grating, thus mapping the pulse's spatial distribution onto a temporal distribution. Because of the increased pulse width, the modulation process discussed in the previous subsection does not need to have a sub-picosecond time scale.

For signal detection purposes, we note that the mapping of space to time due to the pulse tilt can be used to turn temporal change in transmission at the central focal plane into a spatial distribution after the second grating. This is illustrated in Fig. 1(b). Note that the operation is in essence the inverse of what is done in a direct space-to-time pulse shaper [18]. For maximum visibility of the temporal event, all wavelength components should be modulated equally; this also eliminates any possible errors arising from the redirection of the wavelength components by diffraction. If this is the case, the electric field after the second grating is (see Appendix A for derivation)

$$E_{out}(x, t) = E_{in}(x, t)m(t - \gamma x), \tag{7}$$

where $E_{in}(x, t)$ is the input electric field before the first grating, $m(t)$ is the temporal modulation applied by the event, and $\gamma = \lambda_c/(c\Lambda \cos\theta_d)$. Upon detection we integrate the intensity $|E_{out}(x, t)|^2$ over time at each point x. Assuming that the input pulse is free of spatiotemporal dispersion, such that $E_{in}(x, t) = A(x)S(t)$, the spatially resolved signal is the cross-correlation of the local intensity of the input pulse and the amplitude modulation,

$$I(x) = |A(x)|^2 \int |S(t)|^2 |m(t - \gamma x)|^2 dt. \tag{8}$$

Hence, $|S(t)|^2$ acts as a temporal analogue of a point-spread function in traditional incoherent imaging (where though the convolution appears instead of the cross-correlation) [22]. Now considering an event composed of two infinitesimally short events separated by time delay τ such that $m(t) = \delta(t - \tau/2) + \delta(t + \tau/2)$, where $\delta(t)$ is the Dirac delta function, we find

$$I(x) = |A(x)|^2[|S(\gamma x - \tau/2)|^2 + |S(\gamma x + \tau/2)|^2]. \tag{9}$$

Assuming for simplicity $|S(t)|^2 = \mathrm{rect}(t/T_{in})$, we observe that the two events produce rectangular intensity distributions centered around $x_1 = \tau/(2\gamma)$ and $x_2 = -\tau/(2\gamma)$ and having spatial widths of $w_{event} = T_{in}/\gamma$. Clearly, the events are just resolvable if $\tau = T_{in}$. This proves that the time resolution of the system is limited by the temporal width of the input pulse.

Optics EXPRESS

Finally, we note that in the presence of modulation at the central focal plane, any light that is delayed or advanced in time also gains a transverse spatial shift at the output (see the red rectangle in Fig. 1(a)). This shift is equal to

$$\Delta x = \frac{c\Delta t}{\sin(\theta_{\mathrm{d}})}, \tag{10}$$

where Δt is the delay. One can understand this by considering that a delay of Δt corresponds to a spectral phase modulation with a linear phase $\frac{d\phi}{d\omega} = \Delta t$. On the central focal plane, this translates to a linear phase transparency acting as a prism: light is refracted and the propagation direction changes, resulting in a transverse shift of the pulse.

3. Experimental results

Our experimental setup is based on a white-light pump-probe spectroscopy system, shown in Fig. 2. A modelocked Ti:Sapphire laser (Spectra-Physics Tsunami) generates a pulse train (80 fs to 130 fs pulse FWHM, 82 MHz repetition rate) that is chopped using an acousto-optic modulator (AOM) in order to reduce the average power and avoid thermal lensing and photochemical bleaching effects in the sample. A zero-order half-wave plate (HWP) sets the linear polarization state, and is followed by a polarization beam splitter (PBS) that divides the beam into the pump and probe parts. The pump pulse passes through an optical delay line consisting of two mirrors on a piezoelectric motorized stage (New Focus Picomotor). The probe pulse is coupled into a 25 cm long nonlinear optical fiber (NLF) where supercontinuum generation takes place, broadening the probe spectrum. We also insert a half-wave plate in the probe beam to rotate the polarization to match the pump beam polarization. We note that the pump-probe part of the setup is only required to excite the sample with a pump pulse at the appropriate time, and that in general the excitation could come from another source.

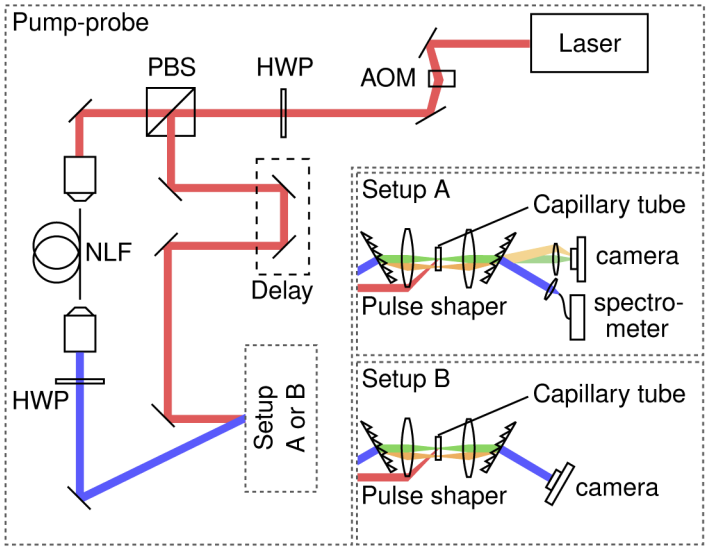

Fig. 2. Experimental setup for all-optical modulation and detection measurements. The setup consists of a pump-probe part, and an experiment-dependent part that consists of the pulse shaper and detectors. The experiments in sections 3.1 and 3.2 use setups A and B, respectively. Initial laser and pump beams are red, while the probe beam is blue. AOM - acousto-optic modulator, HWP - half-wave plate, PBS - polarization beam splitter, NLF - nonlinear fiber.

Optics EXPRESS

The Fourier transform pulse shaper consists of two transmissive, blazed dielectric gratings (Λ = 3300 nm) and two achromatic doublet lenses (focal length 4 cm). The probe beam enters the pulse shaper through the first grating at normal incidence, while the pump beam bypasses the grating. Therefore, the probe pulse is spectrally dispersed at the central focal plane, whereas the pump pulse is focused onto a single spot. The probe beam has a width of 3 mm before the pulse shaper, and thus the temporal pulse width of the probe pulses at the central focal plane is T = 2.3 ps, while the spectral resolution is $\Delta\lambda$ = 0.85 nm. The pump pulse's temporal width is 500 fs (modulation experiment) or 330 fs (detection experiment), limited by material dispersion in the setup. The pump beam is separated from the probe beam, giving it an angle of incidence of 7° at the central focal plane. After the sample, the pump beam is blocked, while the probe beam propagates through the remaining lens and grating to a detector. This can be either a fiber-coupled spectrometer (Ocean Optics USB2000+) for spectral measurements, or a camera (Basler acA1920-25uc with infrared filter removed) to observe the central focal plane through the zeroth diffraction order of the second grating, as shown in Fig. 2. For detection measurements, the camera is moved to detect the first diffraction order immediately after the second grating.

In all-optical modulation experiments, transient spectra are obtained by measuring the spectrum of the probe with and without pumping (resulting in spectra $S(\lambda)$ and $S_{\mathrm{ref}}(\lambda)$, respectively) and then by calculating

$$\frac{\Delta S}{S_{\mathrm{ref}}} = \frac{S(\lambda) - S_{\mathrm{ref}}(\lambda)}{S_{\mathrm{ref}}(\lambda)}, \tag{11}$$

we obtain $\Delta\alpha d = -\ln(1 + \Delta S/S_{\mathrm{ref}})$. The supercontinuum probe permits probing at different wavelengths, but its spectrum is prone to significant pulse-to-pulse fluctuations. This degrades the signal-to-noise ratio because $S(\lambda)$ and $S_{\mathrm{ref}}(\lambda)$ are measured at different times. To combat these fluctuations without requiring a reference measurement of the supercontinuum spectra, we implement a technique inspired by a type of "lucky" imaging [23]. Instead of measuring one spectrum for each of $S(\lambda)$ and $S_{\mathrm{ref}}(\lambda)$ and averaging over a long time to reduce noise, we measure many spectra (20) with short averaging time. We then select a region of the spectrum, which is *not* modulated by the pump beam, and from each group of $S(\lambda)$ and $S_{\mathrm{ref}}(\lambda)$, select the spectra similar to each other in this spectral region. This allows us to reject spectra with large fluctuations and retain those with small fluctuations, significantly improving the signal-to-noise ratio of the transient spectra. This reduces noise in all parts of the spectrum, because the supercontinuum fluctuations at different wavelengths tend to be correlated with each other.

In all experiments we used the dye IR-780 perchlorate (Sigma-Aldrich) dissolved in methanol as the gain medium. The solution was placed in a capillary flow cell consisting of a vertical 100 µm thick rectangular capillary tube (Electron Microscopy Sciences) connected to a small reservoir with the solution flow speed of about 1 cm/s, which prevents thermal distortions and photochemical bleaching (in conjunction with the low average power of the beam).

We calibrated and tested the setup by verifying (using an intensity autocorrelator) that the spectral modulation in the central focal plane of the pulse shaper is properly transferred into temporal modulation. The details of the calibration, utilizing the wavelength-to-time mapping in chirped pulses, are discussed in Appendix B.

3.1. All-optical modulation

In this section, we demonstrate the proposed spectral all-optical modulation by inserting a thin capillary containing IR-780 dye at the central focal plane of the pulse shaper to make use of ground-state depletion and stimulated emission for the modulation effect. In the central focal plane at the position of the capillary dye cell, the pump beam has a spot size of 6 µm, but because it is incident at an angle, it covers a 13 µm transverse distance, corresponding to a 1 nm spectral region. We position the pump to overlap with the probe either at a wavelength of 775 nm for the case of ground-state depletion or at 830 nm for the case of stimulated emission. Then we

Optics EXPRESS

measure the transient spectra of the probe beam as a function of the pump-probe delay. For these measurements, the average power in the pump and probe beams is 0.3 mW and 0.05 mW, respectively. The acousto-optic modulator is used to chop the pulse train into rectangular windows that are 5 µs long, repeating every 1 ms. The pulse energy is about 0.7 nJ and the fluence at the sample is estimated to be $\Gamma = 2.5$ mJ/cm^2 that should be enough to obtain $N_2 \approx 0.43N_0$. The concentration of the IR-780 solution is selected to provide $\alpha d \approx 1$ at the pump wavelength. Hence, we expect $\Delta\alpha d \approx 0.4$.

Figure 3(a) shows the transient spectra at four different pump-probe delays (negative delay means that the pump pulse arrives after the probe pulse). We see that at maximum, we have $\Delta S/S_{\text{ref}} \approx 0.6$, corresponding to $\Delta\alpha d \approx 0.47$. The width of the gain peak is 1.8 nm FWHM, slightly larger than expected. Figure 3(b) shows the peak value of $\Delta S/S_{\text{ref}}$ as a function of the pump-probe delay, where we can observe that, while the excitation happens quickly (< 1 ps), the system then stays in the excited state for several picoseconds, thus affecting the entire 2.3 ps temporal width of the probe. Figures 3(c) and 3(d) show the corresponding plots for the case of stimulated emission, where a smaller $\Delta S/S_{\text{ref}} \approx 0.18$ is obtained ($\Delta\alpha d = 0.2$). The effect is thus weaker, likely a result of non-radiative transitions which deplete the excited states. The decay of the stimulated emission, seen in Fig. 3(d), is rapid (on the order of 1–2 ps). This is thought to relate to transitions into an intermediate state that was observed previously in transient absorption experiments [24]. Nevertheless, the experiment demonstrates that both ground-state depletion and stimulated emission can be used for all-optical modulation in this system. As the spectral width of the supercontinuum probe can be 100 nm or more, and the width of one spectral channel is 1.8 nm, over 50 spectral channels could be individually addressed in this setup. Due to equipment limitations we did not measure the modulation in the time domain. However, the transient spectra show this directly in the frequency domain. Knowing that the initially 80 fs pulse centered at $\lambda = 770$ nm is chirped and is now 500 fs long, the spectral amplitude modulation shown in Fig. 3(a) results in the temporal modulation shown in Fig. 3(e). A 250 fs oscillation is produced in this example, showing the sub-picosecond temporal modulation we wanted to demonstrate.

From the point of view of information transmission, it seems that it would be straightforward to demonstrate THz-bandwidth all-optical modulation and multiplexing with the presented method by picking a higher-repetition-rate laser and improving the spectral resolution. In particular, this could be done in integrated optics where arrayed waveguide gratings [12,25] can be used to construct a pulse shaper with a large number of spectral channels. Furthermore, the power requirements could be lowered by approaching the diffraction limit with higher-numerical-aperture lenses, selecting a gain medium with larger molecular absorption and stimulated-emission cross sections, or enhancing the absorption and emission rates by using micro- or nanostructures [4–7,26,27]. We also note that while in our experiments the pump beam was held stationary, it is actually simple to make it switchable by sending it through the grating together with the signal beam. In this case, the spectrum of the pump will indicate which of the spectral components of the signal are modulated. This can also be done in the integrated optics version proposed above.

3.2. Ultrafast detection

To demonstrate detection with an optical gain medium, we use otherwise the same setup and parameters as with all-optical modulation, except that we reduce the probe beam power until supercontinuum generation stops. The probe beam is then used to obtain a temporal image of the pump pulse. At the position of the dye capillary, the spots of the pump and probe beams overlap at the position of the central wavelength of 770 nm. We thus expect to see ground-state depletion by the pump pulse, which must yield a temporal modulation to the probe pulse. The modulation is then observed in the image of the probe beam taken with the camera. As mentioned earlier, the camera is placed immediately after the second grating at about 3 cm distance. This is far enough

Optics EXPRESS

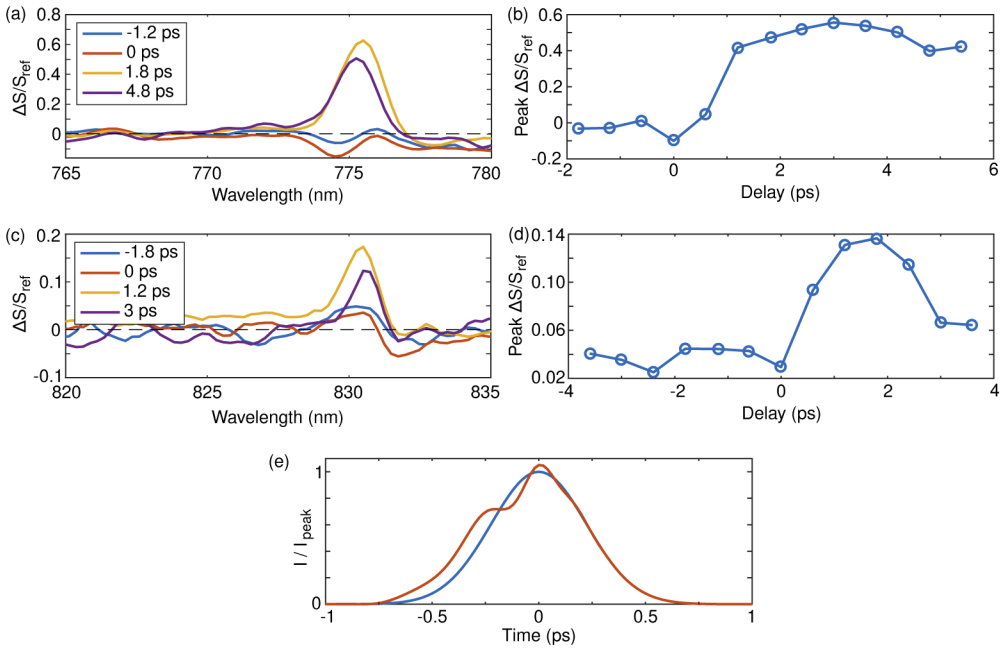

Fig. 3. Spectrally-resolved all-optical modulation: (a) shows transient spectra for different pump-probe delays when the probe at 775 nm is being modulated by the pump-induced ground-state depletion; (b) shows the peak value at 775 nm as a function of the delay; (c) shows transient spectra when the probe beam at 830 nm is modulated by the pump-induced stimulated emission; (d) shows the peak value at 830 nm as a function of the pump-probe delay; (e) shows the calculated intensity as a function of time of the initial and modulated pulses (blue and red curves, respectively) assuming the amplitude modulation from (a).

to let diffraction orders other than the first one to miss the image sensor. Though the camera takes two-dimensional images, the vertical dimension does not hold any temporal or spectral information, and so we average over it to obtain the temporal image [as in Eq. (8)].

We first take a reference image [Fig. 4(a)] by delaying the pump pulse enough not to interact with the probe at all. Because the spatial coordinate in the image plane has a one-to-one correspondence with the temporal coordinate, we present the probe pulse distribution in Fig. 4 as a temporal distribution. We then divide all other images with the reference to take out the effect of the "illumination", that is $|A(x)|^2$ in Eq. (8), leaving only the modulation. Figure 4(b) shows five of these images taken at different arrival times of the pump pulse. In each case the probe beam intensity increases as the pump pulse depletes the population of the ground state [the same phenomenon was observed in Fig. 3(b), but there the time resolution was limited by the 2.3 ps pulse width in the central focal plane]. This intensity increase then allows us to retrieve the pump-pulse duration and profile, similarly to a streak camera [2] but all-optically. As shown by the intervals in Fig. 4(b), the width of the step in the probe intensity increase is 470 fs. Taking into account the finite resolution of the system [the initial pulse width for the probe as in Eq. (8), which is 330 fs], we deduce the duration of the pump pulse to be about 330 fs, as expected; 470 fs is the width of the cross-correlation of two 330 fs Gaussian pulses. The last image in Fig. 4(b) (green curve) is taken with a long delay between the pump (that arrives first) and the probe. This curve is not flat, but exhibits some variation. Likewise, in all curves the part near 2.5 ps exhibits an unphysical decay that was not seen in Fig. 3(b). We believe that the reason for this is that the pump pulse is focused and does not quite cover the whole probe pulse area uniformly. This

Optics EXPRESS

non-uniformity can contribute through pump-pulse-induced lensing effects that arise from the change of refractive index either due to increased temperature or the population inversion. As described earlier we minimized the long-decay thermal effects. Therefore the phase shift due to population inversion seems the most likely explanation for the unexpected behaviour. To achieve the ideal performance analyzed in Section 2, the temporal variation should uniformly cover the probe beam's entire cross section.

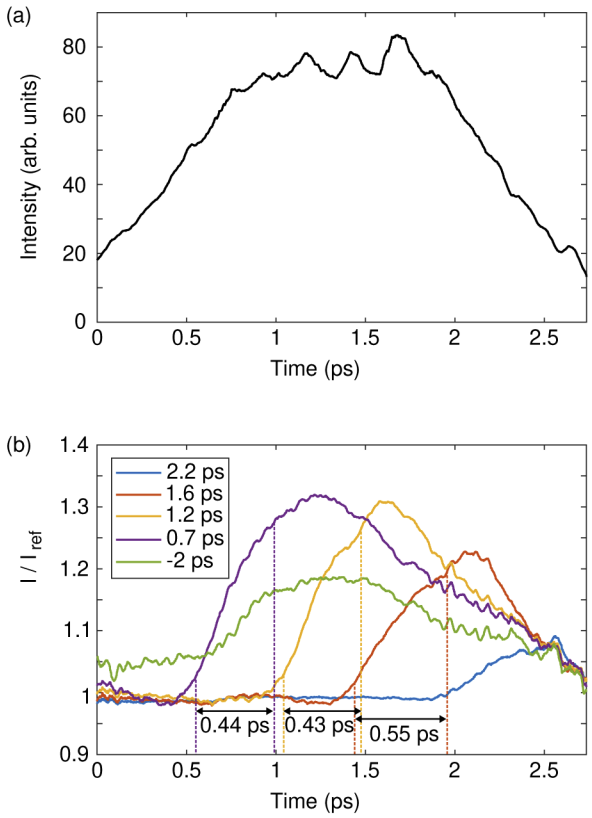

Fig. 4. Ultrafast detection: (a) shows the reference image with no effect from the pump pulse; (b) shows images obtained when the pump pulse partially overlaps with the probe.

The temporally-imaged pump pulse in the current setup had the same spectrum as the probe pulse, which is not required for detection. The only requirement for a pulse to be detected is that it efficiently excites the molecules and depletes the ground state. Furthermore, as shown in Section 2, the time resolution of the system is only limited by the temporal width of the probe pulse. In the present setup we found the resolution to be 500 fs due to the chirp of the pulse, but if the chirp was compensated for, a 80–130 fs transform-limited pulse width (and thus resolution) could be achieved. Furthermore, we obtain a 2.5 ps wide temporal window for the measurement. This can be further increased by either increasing the beam width or using a larger diffraction angle. For example, in this setup, a 1 cm beam width could still be comfortably used, which would lengthen the temporal window up to about 13 ps according to Eq. (6). A window length of 100 ps could be practically achieved with a 5 cm wide diffraction grating at a diffraction angle of 30 degrees, if the probe beam was expanded to fill the whole aperture of the grating.

Optics EXPRESS

4. Conclusions

We demonstrated that by using an optical gain medium, the Fourier-transform pulse shaper becomes a suitable platform for all-optical modulation and detection. First, we showed that the pulse shaper together with a gain medium can be used for all-optical modulation from the viewpoint of both the shaping of optical pulses with other optical pulses and the multiplexing of optical information. A significant advantage of this method is that the underlying modulation mechanism, here the population changes in a gain medium, does not need to act on a sub-picosecond time scale in order to produce sub-picosecond changes in the waveform. It also permits relatively deep (60 % and more) modulation without enhancement by a resonator. One should also bear in mind that more robust gain media, including semiconductors, could be used instead of organic dyes. The device could also be implemented in integrated optics form using arrayed waveguide gratings. In such a format, the proposed all-optical modulators could be used in optical signal processing and telecommunications, in such tasks as multiplexing and demultiplexing, signal regeneration and as parts of optical logic gates.

Second, we proposed, analyzed and demonstrated a gain-medium-assisted ultrafast signal detection technique. The method has a high temporal resolution, limited only by the width of the illumination pulse, and it can reach quite long burst times. It therefore shares many benefits of chirped-pulse and time-lens techniques, while also being simple to implement.

A. Output electric field in ultrafast detection

We modify the theory of Ref. [14] to describe the electric field of the output pulse when the pulse is modulated temporally at the central focal plane of the pulse shaper. In the frequency domain, the electric field at the central focal plane before modulation is

$$E_3(x,f') = \tilde{E}_{\text{in}}(\frac{x}{\lambda_c L} - f'\gamma, f'), \tag{12}$$

where $f' = f - f_c$ with f_c being the central frequency, $\tilde{E}_{\text{in}}(f_x,f')$ is the spatial Fourier transform of the input pulse electric field just before the first grating of the pulse shaper, λ_c is the central wavelength, and $\gamma = \lambda_c/(c\Lambda\cos\theta_d)$. Applying the temporal modulation $m(t)$ is equivalent to convolving Eq. (12) with the temporal Fourier transform of $m(t)$. The resulting electric field is

$$E_4(x,f') = \int E_3(x,f'')\hat{m}(f' - f'')df''. \tag{13}$$

Then, the electric field at the output (after the second grating) is

$$E_5(x,f') = \int E_4(\lambda_c L[f_x + f'\gamma], f')e^{i2\pi f_x x}df_x, \tag{14}$$

which after simplification and a temporal inverse Fourier transform yields

$$E_5(x,t) = E_{\text{out}}(x,t) = E_{\text{in}}(x,t)m(t - \gamma x). \tag{15}$$

B. Frequency-to-time mapping in chirped pulses

We experimentally verified the wavelength-to-time mapping in spectrally modulated chirped pulses used in our system and its suitability for pulse shaping. In chirped pulses, modulation of the spectrum is transferred directly to the time domain. Though slightly more limited than the methods of "arbitrary" shaping of unchirped pulses, the proposed method has the advantage of being nearly free of transverse spatial shifts that usually appear at the pulse shaper output. It could therefore be useful for the creation of long pulse trains without disturbing the beam quality

Optics EXPRESS

and power efficiency, which is difficult to achieve with existing shapers of both the ordinary Fourier-transform [13] and the direct-space-to-time [18] type.

In a chirped optical pulse, the spectrum of the pulse is (partially) mapped into the time domain as different wavelength components are delayed with respect to each other. Assuming that only second-order dispersion is present and that the pulse's spectral width satisfies $\Delta\lambda_{\mathrm{tot}} << \lambda_{\mathrm{c}}$, the time delay for the wavelength λ can be written as

$$\tau = Dz(\lambda - \lambda_{\mathrm{c}}), \tag{16}$$

where D is the dispersion parameter and z is the length of the dispersive element. This time-to-wavelength mapping was exploited for temporal imaging in the SF-STAMP technique [11]. Here we apply the same principle to pulse shaping. Essentially, the spectrum is divided into sub-spectra, each having a full width at half maximum of $\Delta\lambda_{\mathrm{sub}}$, and each sub-spectrum is used to form a sub-pulse in the time domain. If the initial pulse is Gaussian and has a FWHM spectral width $\Delta\lambda_{\mathrm{tot}}$, the temporal width (FWHM) of each sub-pulse is

$$\tau = \sqrt{\left(\frac{2\lambda_{\mathrm{c}}^2 \ln 2}{\pi c \Delta\lambda_{\mathrm{sub}}}\right)^2 + (Dz\Delta\lambda_{\mathrm{sub}})^2}. \tag{17}$$

For a given value of Dz, this has a minimum at

$$\tau_{\mathrm{min}} = 2\sqrt{\frac{Dz\lambda_{\mathrm{c}}^2 \ln 2}{\pi c}}, \tag{18}$$

for which

$$\Delta\lambda_{\mathrm{sub}} = \sqrt{\frac{2\lambda_{\mathrm{c}}^2 \ln 2}{\pi c Dz}}. \tag{19}$$

The number of sub-pulses of length τ_{min} that can be independently created is

$$N = \frac{\Delta\lambda_{\mathrm{tot}}}{\Delta\lambda_{\mathrm{sub}}}. \tag{20}$$

Choosing the optimal values and tuning Dz, one can obtain either a few short sub-pulses or many long sub-pulses.

This technique cannot reach the resolution limit achieved with spectral modulation at a given spectral width. However, it does have an interesting advantage for applications where it would be desirable to have long time delays between the sub-pulses. As revealed by Eq. (10), normally creating a sub-pulse at time delay τ results in a transverse shift, and as a result, the beam quality can suffer unless the beam is very large in diameter to begin with. For example, even in the best case of $\sin\theta_{\mathrm{d}} \rightarrow 1$ the transverse shift for a 10 ps delay would be 3 mm. However, when using a chirped pulse, temporal modulation can be obtained without any noticeable transverse shifts of the pulse profile. Furthermore, the technique shares with space-to-time pulse shapers the convenience of one-to-one mapping between the spatially addressed modulation and the time domain, while achieving high efficiency.

For experimental verification, we only consider the probe beam input to the pulse shaper (the blue beam in Fig. 2), and in addition to the camera and spectrometer, we use an intensity autocorrelator (Femtochrome FR-103XL) to measure the pulses in the time domain. The autocorrelator's nonlinear crystal has a limited bandwidth for phase matching, and allows us to observe proper intensity autocorrelation only for fields with a small chirp. Otherwise, considering some central wavelength λ_{c}, a sub-pulse at wavelength $\lambda_{\mathrm{c}} + \Delta\lambda$ is phase-matched with another sub-pulse at $\lambda_{\mathrm{c}} - \Delta\lambda$, producing a side peak in the autocorrelation function. Phase matching

Optics EXPRESS

of $\lambda_c + \Delta\lambda$ with itself (contributing to the central peak of the autocorrelation function) is weak, and thus the central part is suppressed. Hence, to show the effect of spectral modulation on the time-domain behaviour of a chirped pulse, we perform two experiments. First, we substantially limit the spectrum and then modulate a part of it to show that modulation at a given wavelength is properly manifested in the time domain. Second, we divide the spectrum into two to create two sub-pulses, showing the relationship between time and frequency and the resolution of the system. The known parameters of the setup are the dispersion $Dz = 50$ ps/nm, central wavelength $\lambda = 770$ nm, and laser pulse spectral width $\Delta\lambda_{tot} = 10$ nm. Using Eqs. (18)–(20) we also obtain $\tau_{min} = 300$ fs, $\Delta\lambda_{sub} = 4.2$ nm and $N = 2.5$. We therefore expect to be able to create at least two sub-pulses in the present case.

In the first experiment we use a 50 µm wide slit in the central focal plane to limit the spectrum, and then insert a thin metal wire at the center of the slit. The wire is 20 µm wide. Figure 5(a) shows the intensity distribution of the probe beam at the central focal plane without and with the blocking wire (blue and red curves, respectively); the amplitude modulation is clearly visible. The inset shows the same intensity distribution in the two-dimensional plane. As expected, this is directly translated into the spectrum, shown in Fig. 5(b). The spectral features are smoother than

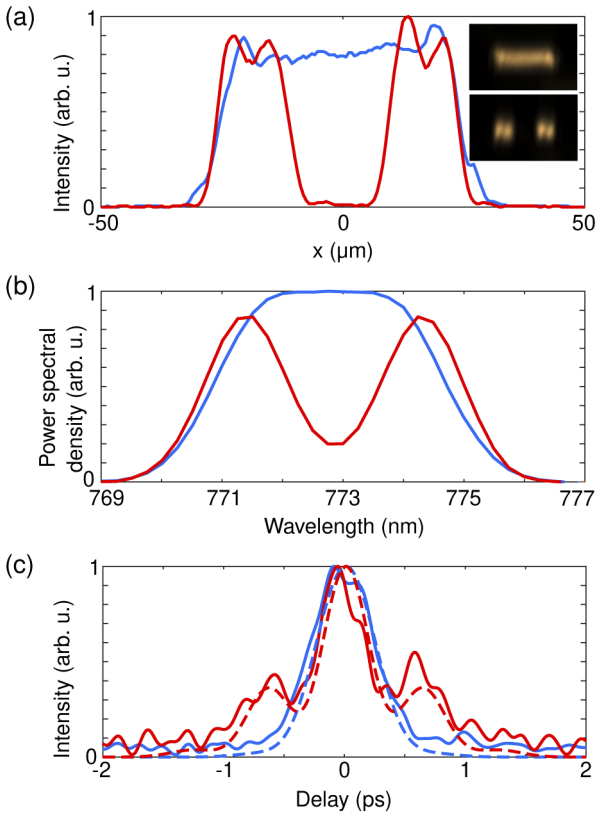

Fig. 5. Narrowband modulation. In all plots, the solid blue and red curves correspond to measurements taken before and after blocking the central part of the pulse, respectively. The intensity at the central focal plane of the pulse shaper is shown in (a) as a function of the transverse coordinate. The inset shows two-dimensional intensity distributions without and with modulation in the central part. The measured spectra are shown in (b). The intensity autocorrelation functions are shown in (c), where the dashed curves correspond to theoretical calculations.

Optics EXPRESS

the spatial intensity modulation due to the limited spectral resolution of the pulse shaper. Finally, Fig. 5(c) shows the autocorrelation function, where without the wire (solid blue curve) we have a single peak with a FWHM of 620 fs, whereas with the wire (solid red curve) we obtain two side peaks at 700 fs delay, corresponding to the period of the beating of two waves at 2.75 nm wavelength separation. The result fits well with the theoretical prediction shown by the dashed blue and red curves (without and with the wire, respectively), which was calculated by using the known parameters of the input pulse and applying the spectral amplitude modulation shown in Fig. 5(b). This proves that spectrally narrow modulation works properly in the system.

In the second experiment, we use two slits, each 25 µm wide and with a center-to-center separation of 145 µm. Figure 6(a) shows the intensity distribution at the central focal plane, and Fig. 6(b) shows the measured spectrum that this time consists of two 2.5 nm wide peaks separated by 12 nm. With the chirp factor Dz = 50 fs/nm we expect to see two pulses of 450 fs FWHM separated by 600 fs. Figure 6(c) shows the autocorrelation function with the side peaks indeed corresponding to a 600 fs delay, thus confirming the expected operation of the system. The central part of the autocorrelation function is suppressed due to the phase mismatch discussed above. The theoretically predicted autocorrelation function has shoulders at the positions corresponding to the side peaks of the experimental autocorrelation function.

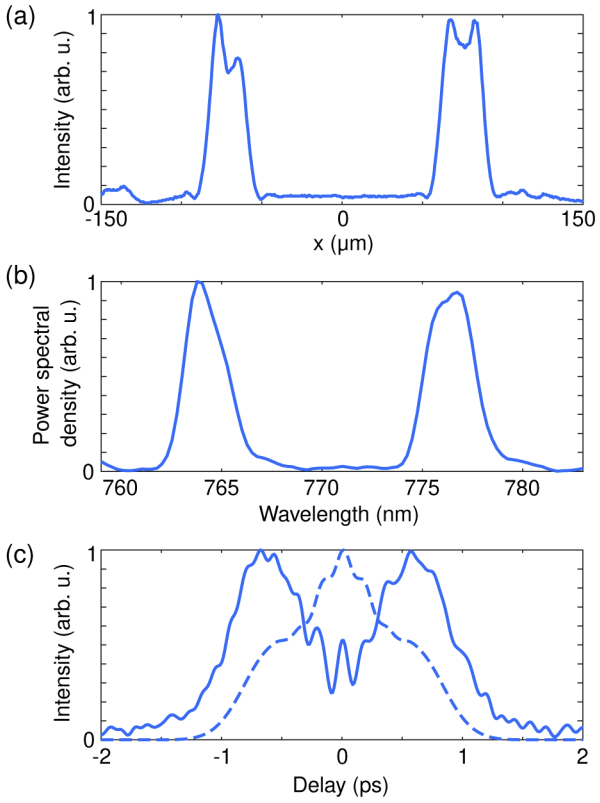

Fig. 6. Creation of sub-pulses: (a) shows the spatial intensity distribution at the central focal plane, (b) illustrates the spectrum, and (c) shows the measured autocorrelation function (note that the central part of the function is missing due to the discussed phase-matching issues). The dashed line in (c) shows the theoretical prediction.

These experiments show that the system operates as an efficient chirped-pulse modulator with the achievable intra-pulse modulation rate exceeding 1 THz and an almost one-to-one mapping

Optics EXPRESS

between the spectral and time modulations. As predicted in Sec. 2 theoretically, we do not see any noticeable distortion in the beam profile at the pulse shaper output.

Funding

Suomen Kulttuurirahasto (00190768); Academy of Finland (308394).

Acknowledgments

We also acknowledge the Academy of Finland Flagship Programme, Photonics Research and Innovation (PREIN).

Disclosures

The authors declare no conflicts of interest.

References

1. P. Minzioni, C. Lacava, T. Tanabe, J. Dong, X. Hu, G. Csaba, W. Porod, G. Singh, A. E. Willner, A. Almaiman, V. Torres-Company, J. Schröder, A. C. Peacock, M. J. Strain, F. Parmigiani, G. Contestabile, D. Marpaung, Z. Liu, J. E. Bowers, L. Chang, S. Fabbri, M. R. Vázquez, V. Bharadwaj, S. M. Eaton, P. Lodahl, X. Zhang, B. J. Eggleton, W. J. Munro, K. Nemoto, O. Morin, J. Laurat, and J. Nunn, "Roadmap on all-optical processing," J. Opt. **21**(6), 063001 (2019).
2. J. Liang and L. V. Wang, "Single-shot ultrafast optical imaging," Optica **5**(9), 1113–1127 (2018).
3. Mikami Hideharu, Gao Liang, and Goda Keisuke, "Ultrafast optical imaging technology: Principles and applications of emerging methods," Nanophotonics **5**(4), 497–509 (2016).
4. B. T. Diroll, K. S. Schramke, P. Guo, U. R. Kortshagen, and R. D. Schaller, "Ultrafast Silicon Photonics with Visible to Mid-Infrared Pumping of Silicon Nanocrystals," Nano Lett. **17**(10), 6409–6414 (2017).
5. K. Nozaki, T. Tanabe, A. Shinya, S. Matsuo, T. Sato, H. Taniyama, and M. Notomi, "Sub-femtojoule all-optical switching using a photonic-crystal nanocavity," Nat. Photonics **4**(7), 477–483 (2010).
6. M. R. Shcherbakov, P. P. Vabishchevich, A. S. Shorokhov, K. E. Chong, D.-Y. Choi, I. Staude, A. E. Miroshnichenko, D. N. Neshev, A. A. Fedyanin, and Y. S. Kivshar, "Ultrafast All-Optical Switching with Magnetic Resonances in Nonlinear Dielectric Nanostructures," Nano Lett. **15**(10), 6985–6990 (2015).
7. Y. Yang, K. Kelley, E. Sachet, S. Campione, T. S. Luk, J.-P. Maria, M. B. Sinclair, and I. Brener, "Femtosecond optical polarization switching using a cadmium oxide-based perfect absorber," Nat. Photonics **11**(6), 390–395 (2017).
8. C. Koos, P. Vorreau, T. Vallaitis, P. Dumon, W. Bogaerts, R. Baets, B. Esembeson, I. Biaggio, T. Michinobu, F. Diederich, W. Freude, and J. Leuthold, "All-optical high-speed signal processing with silicon–organic hybrid slot waveguides," Nat. Photonics **3**(4), 216–219 (2009).
9. R. Bruck, K. Vynck, P. Lalanne, B. Mills, D. J. Thomson, G. Z. Mashanovich, G. T. Reed, and O. L. Muskens, "All-optical spatial light modulator for reconfigurable silicon photonic circuits," Optica **3**(4), 396–402 (2016).
10. L. Lundberg, M. Karlsson, A. Lorences-Riesgo, M. Mazur, V. Torres-Company, J. Schröder, and P. A. Andrekson, "Frequency Comb-Based WDM Transmission Systems Enabling Joint Signal Processing," Appl. Sci. **8**(5), 718 (2018).
11. T. Suzuki, F. Isa, L. Fujii, K. Hirosawa, K. Nakagawa, K. Goda, I. Sakuma, and F. Kannari, "Sequentially timed all-optical mapping photography (STAMP) utilizing spectral filtering," Opt. Express **23**(23), 30512–30522 (2015).
12. A. Vega, D. E. Leaird, and A. M. Weiner, "High-speed direct space-to-time pulse shaping with 1 ns reconfiguration," Opt. Lett. **35**(10), 1554–1556 (2010).
13. A. M. Weiner, "Femtosecond pulse shaping using spatial light modulators," Rev. Sci. Instrum. **71**(5), 1929–1960 (2000).
14. M. Wefers and K. Nelson, "Space-time profiles of shaped ultrafast optical waveforms," IEEE J. Quantum Electron. **32**(1), 161–172 (1996).
15. E. Frumker and Y. Silberberg, "Femtosecond pulse shaping using a two-dimensional liquid-crystal spatial light modulator," Opt. Lett. **32**(11), 1384–1386 (2007).
16. E. Frumker, E. Tal, Y. Silberberg, and D. Majer, "Femtosecond pulse-shape modulation at nanosecond rates," Opt. Lett. **30**(20), 2796–2798 (2005).
17. A. M. Weiner and D. E. Leaird, "Generation of terahertz-rate trains of femtosecond pulses by phase-only filtering," Opt. Lett. **15**(1), 51–53 (1990).
18. D. Leaird and A. Weiner, "Femtosecond direct space-to-time pulse shaping," IEEE J. Quantum Electron. **37**(4), 494–504 (2001).
19. M. A. Foster, R. Salem, D. F. Geraghty, A. C. Turner-Foster, M. Lipson, and A. L. Gaeta, "Silicon-chip-based ultrafast optical oscilloscope," Nature **456**(7218), 81–84 (2008).

Optics EXPRESS

20. C. Ruckebusch, M. Sliwa, P. Pernot, A. de Juan, and R. Tauler, "Comprehensive data analysis of femtosecond transient absorption spectra: A review," J. Photochem. Photobiol., C **13**(1), 1–27 (2012).
21. A. Shevchenko, P. Ryytty, T. Kajava, M. Hautakorpi, and M. Kaivola, "Single-longitudinal-mode selection in a nanosecond-pulsed dye laser," Appl. Phys. B: Lasers Opt. **74**(4-5), 349–354 (2002).
22. B. E. A. Saleh and M. C. Teich, *Fundamentals of Photonics*, 2nd ed. (Wiley, 2007).
23. D. L. Fried, "Probability of getting a lucky short-exposure image through turbulence," J. Opt. Soc. Am. **68**(12), 1651–1658 (1978).
24. D. K. Das, K. Makhal, and D. Goswami, "Observing ground state vibrational coherence and excited state relaxation dynamics of a cyanine dye in pure solvents," Phys. Chem. Chem. Phys. **20**(19), 13400–13411 (2018).
25. A. Krishnan, L. G. de Peralta, V. Kuryatkov, A. A. Bernussi, and H. Temkin, "Direct space-to-time pulse shaper with reflective arrayed waveguide gratings and phase masks," Opt. Lett. **31**(5), 640–642 (2006).
26. P. Biagioni, J.-S. Huang, and B. Hecht, "Nanoantennas for visible and infrared radiation," Rep. Prog. Phys. **75**(2), 024402 (2012).
27. M. Nyman, A. Shevchenko, I. Shavrin, Y. Ando, K. Lindfors, and M. Kaivola, "Large-area enhancement of far-field fluorescence intensity using planar nanostructures," APL Photonics **4**(7), 076101 (2019).